Supplementary Information

Reducing the Structural Mass of Large Direct Drive Wind Turbine Generators Through Triply Periodic Minimal Surfaces Enabled by Hybrid Additive Manufacturing

Authors: Austin C. Hayes and Gregory L. Whiting

List of Figures

List of Tables

Genetic Algorithm

The genetic algorithm variant shown in Fig. S2 depicts the algorithmic process for selecting more optimal rotor designs. The main variant in this design was the introduction of outside species for increased randomness. This helped prevent the GA from becoming stuck on local minima. However, the effectiveness of this technique decreases as the solution progresses as the liklihood of random chance producing a better solution than the GA decreases with increasing generations. Therefore, a better solution may exist after the GA hits its lowest local minima. Nevertheless, this technique proved effective at greatly improving the mass and deflections of the designs.

A mesh analysis was performed in order to ensure the correct balance between computational efficiency and physics representation was achieved. For each GA design and strain field optimized design, progressive reduction in the mesh size was performed and the resulting torsional deflection plotted. An asymptotic approach to a value indicates a fine enough mesh to resolve deflections. It should be noted that due to reduced thicken and thin lattice thicknesses, the strain field optimization required a finer mesh than the genetic algorithm.

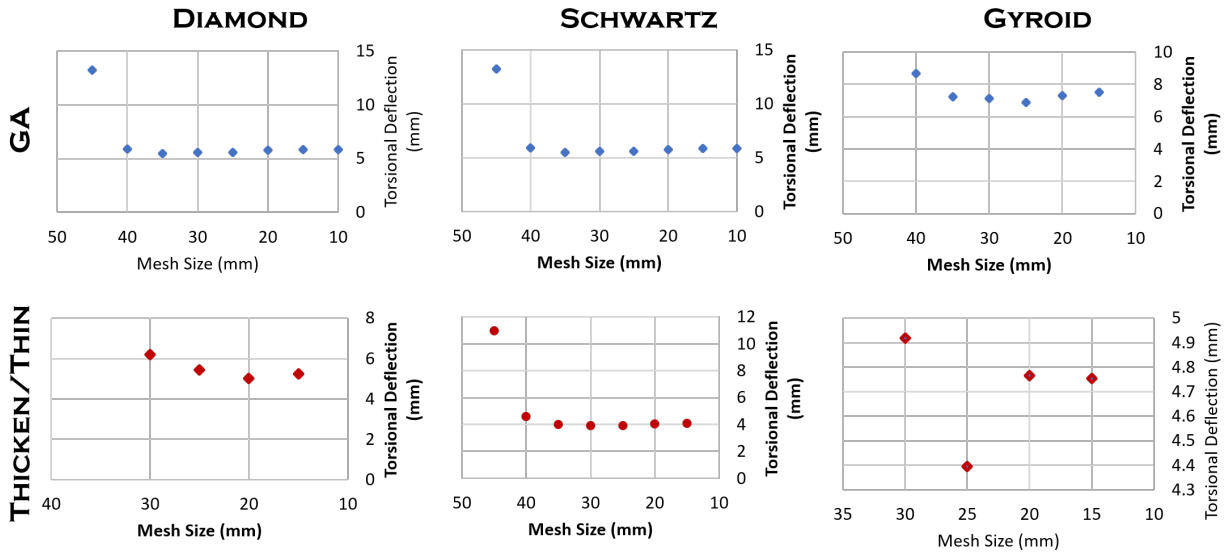

Figure S1: Mesh analysis for FEA torsional deflection of GA and strain optimized final designs for a 5 MW rotor

Justification of the genetic algorithm by comparison with random sampling is seen in Fig. S3. For the genetic algorithm to be useful in reducing computations needed to improve the solution, it must achieve quicker convergence to a minima than randomly sampling. In this study, random sampling of the Schwartz rotor design space resulted in a lowest fitness score of 8.823 versus the GA result of 7.142. This reflects a structural mass of 10,500 kg and unacceptable torsional deformation of 10.25 mm compared to the GA result of 10,900 kg with 3.88 mm torsional deformation.

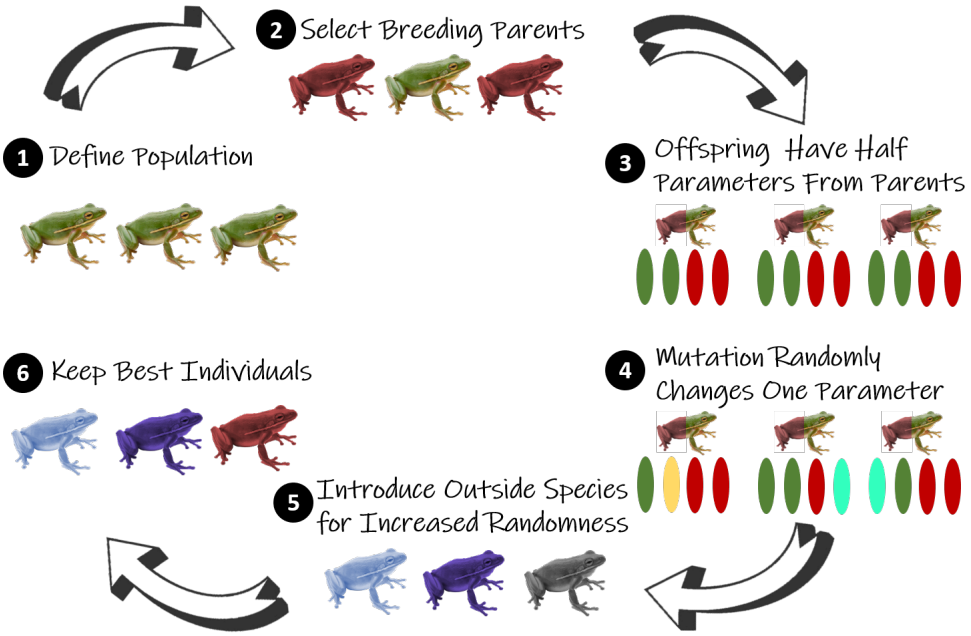

Figure S2: Genetic Algorithm Variant

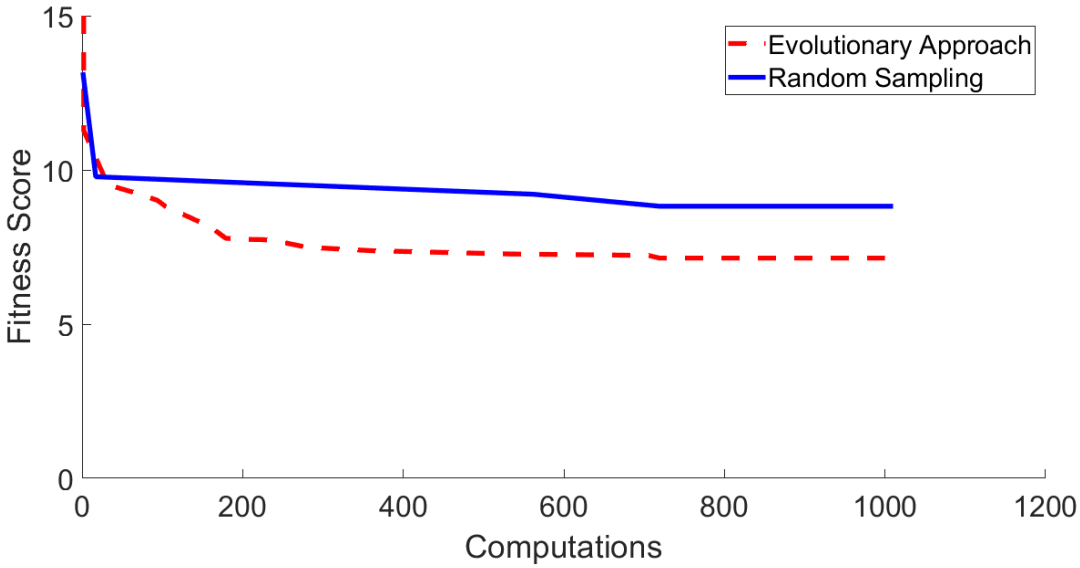

Figure S3: Evolutionary Algorithm Versus Random Sampling

PLA Material Properties

The stress-strain curve for PLA dogbones printed on a Raise 3D FDM printer are shown in Fig. S4. The slopes agree with one another and the advertised elastic modulus of a 100% infill PLA part was 2.636 GPa which agreed with experimental results.

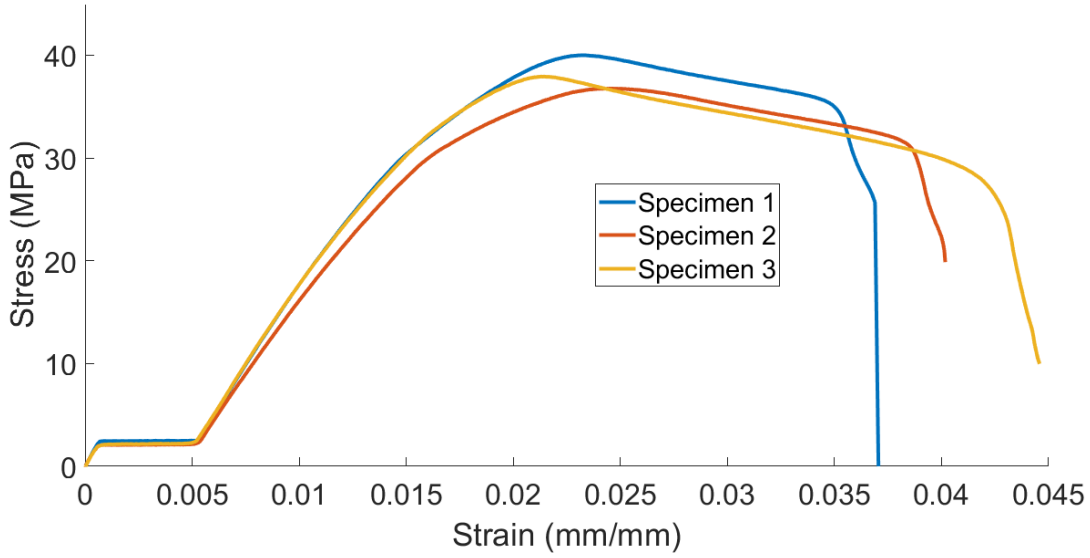

Figure S4: Stress Strain Curve for PLA at 100% Infill

Cast Rotor Designs

Investment casting of complex TPMS structures was successfully completed with lost-wax casting of a printed part. A traditional investment casting process was carried out for three TPMS structures of varying complexity to determine the ability of casting to manufacture these complex geometries. All three rotor designs were successfully cast out of bronze at the Art Castings of Colorado.

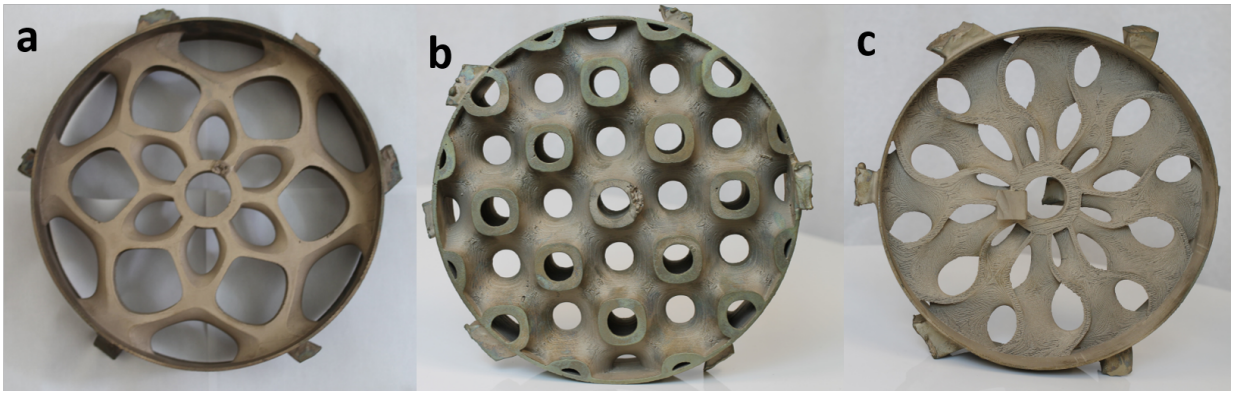

Figure S5: (a) Cast Schwartz Cylindrical Rotor (b) Cast Schwartz Cartesian Rotor (c) Cast Gyroid Cylindrical Rotor

PLA Rotor for DIC Analysis

In order to perform digital image correlation comparison to FEA, a known force must be applied to the rotor. Due to the difficulty to mimic exact loading conditions by placing magnets around the circumference

and creating a stator, a torque arm was added to the design to produce a force by hanging a known weight off the arm. The torque arm was printed as one piece on the rotor in order to eliminate interface effects. Furthermore, a shaft was also printed as one piece for the same reason. This enabled an isotropic model of PLA to be used which facilitated easy comparison to the FEA model. An image of the printed rotor for DIC analysis can be found in Fig. S6.

Figure S6: PLA printed Schwartz Primitive rotor for DIC analysis with shaft and torque arm

DIC Results Inner Ring

Due to distortion effects of the image, the outer radius of the DIC results are less accurate than the inner radius. This helps explain differences in deflection between FEA and DIC at the lower outer radius values. However, FEA and DIC results agree in trend with the shaft deflection at 0 mm and deflections increasing symmetrically radially outward from the center of the rotor ring. A stress concentration occurs at the interface of the torque arm and the rotor confirmed in both FEA and DIC. Furthermore, a point selected within the lattice geometry depicted an 84 μm difference between the FEA results and DIC. As the pixel resolution was 83 μm, this suggests agreement within error.

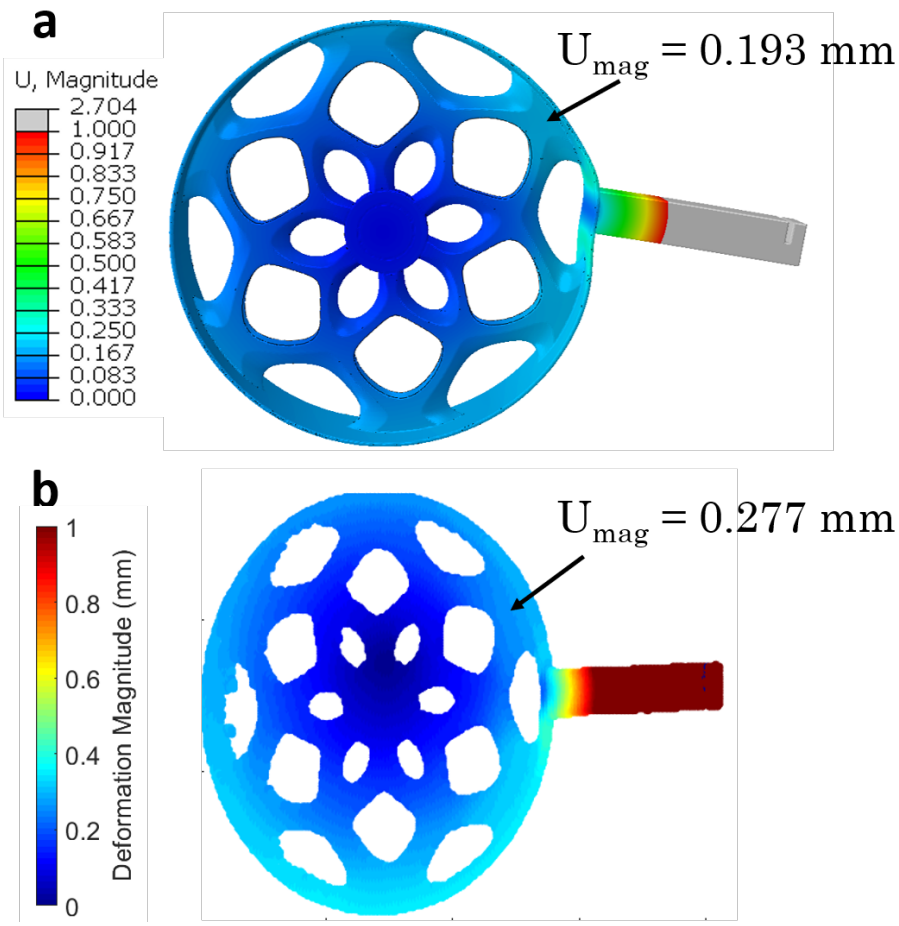

Figure S7: (a) Abaqus simulation results for Schwartz Primitive design showing inner ring deformations (b) DIC analysis results for Schwartz Primitive design showing inner ring deformations